Iraqi J. Laser, Issue (1), Vol.18, pp.13-23 (2019)

IRAQI JOURNAL OF LASER

Design and Implementation Tunable Band Pass Filter based on PCF-Air Micro-cavity FBG Fabry-Perot Resonator

Faraqid Q. Mohammed[(1)] and **Tahreer S. Mansour**[(2)]

(1) Ministry of ministry of industry and minerals, Baghdad, Iraq
(2) Institute of Laser for Postgraduate Studies, University of Baghdad, Baghdad, Iraq

(Received 6 September 2018; accepted 23 September 2018)

Abstract: A tunable band pass filter based on fiber Bragg grating sensor using an in-fiber Mach-Zender interferometer with dual micro-cavities is presented. The micro-cavity was formed by splicing together a conventional single-mode fiber and a solid core photonic crystal fiber (SCPCF) with simple arc discharge technique. Different parameters such as arc power, length of the SCPCF and the overlap gap between samples were considered to control the fabrication process. The ellipsoidal air-cavity between the two fibers forms Fabry-Perot cavity. The diffraction loss was very low due to short cavity length. Ellipsoidal shape micro-cavities were experimentally achieved parallel to the propagation axis having dimensions of (24.92 – 62.32) µm of width and (3.82 – 18.2) µm of length. The maximum tunability 0.73nm was achieved at minimum length of (SCPCF) in the range (1545.673-1545.546) nm. A micro-cavity with width and length as high as 62.32 um and 18.3 um have higher sensitivity 0.31 nm/cm than temperature sensitivities of 18 pm/°C.

Keywords: Fiber Bragg Grating (FBG), Fabry Perot interferometer, (FPI), Photonic crystal fiber (PCF), Large, Mode Area (LMA-10), tunable filter.

Introduction

Optical fiber sensors (OFSs) have been developed and used broadly for physical and chemical measurement such as strain, temperature, pressure, and reflective index. OFSs bear important features such as intrinsic safety, resistance to chemical corrosion, immunity to electromagnetic interference, electric isolation, small size, lightweight sensing heads, high resolution, easy multiplexing, and capability for extremely remote monitoring [1, 2]. Among the OFSs, fiber Bragg gratings (FBG) backscattered spectrum shifts are by far the most used for measuring temperature and/or mechanical strain [3,4]. Nonetheless, interrogation system is the most important drawback for their large commercial application, due to their high cost. Therefore, the development of new, and lower cost, interrogation alternatives are essential [5]. FBG sensor spectrum is usually monitored either by an optical spectrum analyzer (OSA) or a commercial FBG interrogator system. For real-time application in industry, the OSA is not suitable due to tradeoffs between resolution and sweep frequency; not to mention OSA cost, volume and weight [6]. Commercial OFS interrogators (designed based on scanning laser or scanning filters) are able to probe the FBG spectrum with higher resolution. But, they become extremely expensive whenever

hundreds scans per second are required [7, 8]. In this paper, we demonstrated a new approach of design and implementation a tunable band pass filter by introducing two identical FBGs with a dual, ellipsoidal shape, micro-cavities PCFs using fusion splicing, of PCF type LMA-10 with standard single mode fiber SMF-28. A careful adjustment of splicing parameters have accurately considered to reach higher tunability.

Fabrication and Analytical modeling

This section provides a precise and clear demonstration of sensor fabrication process and the experiment procedures and parameters followed in this manuscript.

Micro-cavity construction

A manual splicing mode of fusion splicing machine Fujikura type FSM-60S stated in datasheet reference [9] has been used to perform the fabrication process. A 1.5 cm length of PCF type LMA – 10 has been prepared and spliced with 30 cm length of SMF-28s as shown in figure (1). To accomplish an optimum splicing between both fibers, first, the coating layer was stripped using alcohol solution. Second, both fibers were perpendicularly cleaved to the longitudinal axis of the fiber. This is a crucial step have to be maintained to ensure maximum light coupling between both segments. Third, both fibers were spliced based to optimum parameters of the device. The formation of micro-cavity inside LMA-10 PCF is governed by numbers of parameters. These parameters are split into geometrical and machine parameters. Geometrical parameters play a significant role for micro-cavity formation. They are related, in one hand, to the geometrical shape of the used optical fiber, the length of the segment, air holes distribution and the happening collapse during the splicing procedure. On the other hand, splicing parameters such as arc power, arc time, offset and overlap between aligned samples are also affecting the preparation process which they are the major factors of the air holes collapsing as stated in [10-13] and the air cavity formation. Different sizes of micro-cavities were maintained based on changing the arc fusion power, arc fusion time, overlap and the gap. All values taken to achieve this step are tabulated in table (1)

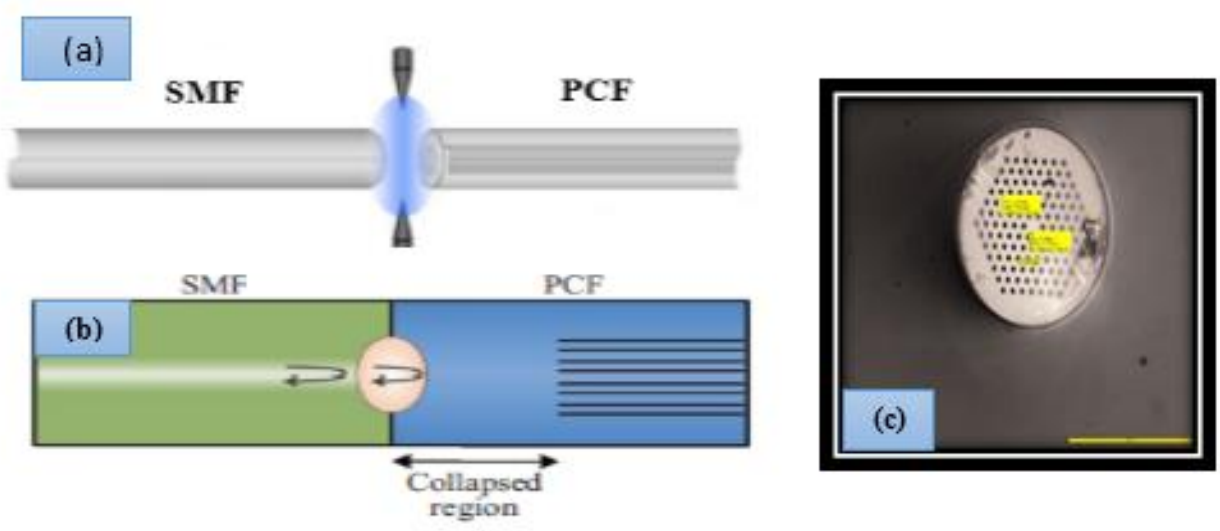

Fig. (1): (a) Schematic diagram of splicing PCF to SMF [13] (b) Micro - cavity formed at the junction between SMF and SCPCF (LMA-10) [14] (C) Cross section of LMA-10 from microscope in laboratory.

Table (1): Fusion splicing parameters for construct micro-cavity.				
splicing parameter LMA-10 to SMF	**Settings 1**	**settings 2**	**settings 3**	**settings 4**
Perfusion time (ms)	1000	1000	1000	1000
Perfusion power (bit)	STD-10	STD-20	STD-30	STD-40
Arc power (bit)	50	40	30	20
Overlap(μm)	5	8	5	8
Gap (μm)	15	10	15	10

Two sensors were fabricated using fusion splicing technique. The arc power and arc time were optimized to maintain and justifying collapse with arbitrary holes shape at the junction between both fibers as shown in figure(2).

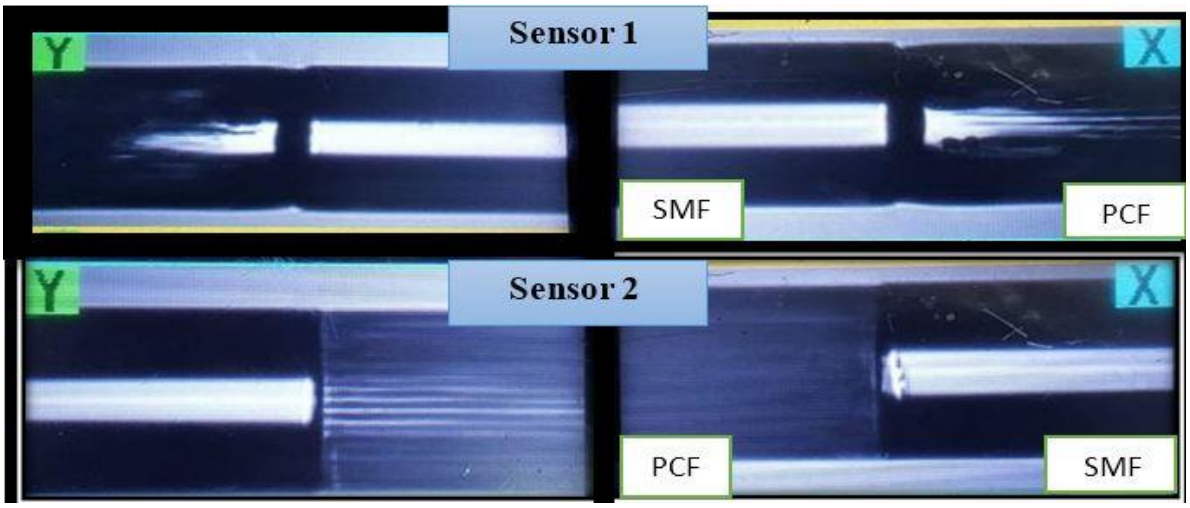

Fig . (2): Splicing point between SMF and PCF at both sides for the proposed sensor.

Formation MZI with dual micro-cavity

The micro-cavity was fabricated from air in this paper. It has spherical shape where r =d or ellipsoidal shape where r > d. Air micro-cavity embedded in fiber whose diameter is 2R as shown in figure (3).

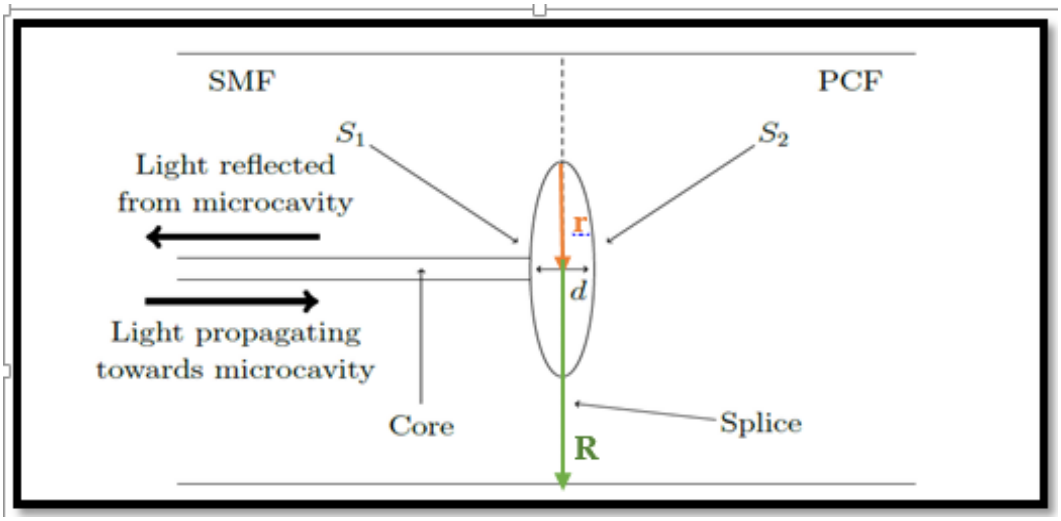

Fig. (3): Diagram of ellipsoidal shape micro-cavity at the splicing joint with two reflecting surfaces S1 and S2 are appeared at opposite sides of the two spliced optical fibers [19].

Ellipsoidal shape of the micro-cavity rotated around its minor axis, with size of (2dx2r), in which 2d is the polar diameter and r is the radius. The ellipsoidal polar axis was coincided with the path of light propagation. Air micro-cavity acts like a Fabry - Perot etalon where the incident light propagated along the fiber core encounter the first silica - air interface (S_1) and reflected due to Fresnel reflection. It coupled with the light reflected from the second interface air- silica (S_2) backward into the SMF. The intensity of light was given by [15]

$$I=I_1+I_2+2\sqrt{I_1\ I_2}cos\Delta\phi \quad (1)$$

Where I_1 and I_2 are the intensities of the of reflection of S_1, S_2 respectively

$\Delta\phi$ is the phase difference between the two reflected light beams, given by

$$\Delta\phi = \frac{4\pi\,\Delta n_{eff} L}{\lambda} + \pi \quad (2)$$

Where λ is the operating wavelength and Δn_{eff} is the effective refractive index difference between the core and cladding mode, it can be given as [16].

$$\Delta n_{eff} = n_{eff}^{\ core} - n_{eff}^{\ cladding} \quad (3)$$

The m-order resonance wavelength can be given as

$$\lambda_m = \frac{2\left(n_{eff}^{core} - n_{eff}^{cladding}\right)L}{2m+1} = \frac{2n_{eff}L}{2m+1} \quad (4)$$

The hybrid structured in-line MZI is composed of an embedded slender air cavity in both side of PCF as shown in figure (4) [17].when light pass through the SMF in to micro-cavity 1, part of light in SMF core will be coupled in to higher order cladding modes because of different refractive index between core and cladding of PCF. The free spectral range of the fabricated MZI was expressed as*:*

$$FSR = \lambda_{m-1} - \lambda_m = \frac{\lambda m\ \lambda_{M-1}}{n_{eff}\,L} \quad (5)$$

Construction band Pass Filter Based on FBG and MZI with dual micro-cavities

A photosensitive single mode fiber (ThorLabs) was used to record the uniform FBG sensor using the phase mask technique. A 15mm length FBG was selected to get more than 90% of reflectivity. In order to analyze the behavior of the proposed system, an analytical modeling for the system composed by both micro-cavity and FBG is presented. The FPI can be considered as an optical resonator which consists of a 2 plane-parallel (two identical FBGs) reflecting surfaces (mirrors) with reflectivity (R) separated with a short segment SCPCF contained the air micro-cavity with different dimension. The round-trip optical phase delay between the back reflected signals is giving by [17].

$$\varphi = \frac{4\pi n_{pcf} L_{pcf}}{\lambda} \quad (6)$$

Where n_{pcf} is the effective index, L_{pcf} is the cavity length and λ is the operating wavelength. For SCF L_{pcf}= 1.5 cm. In this case, the incidence is considered normal so $\varphi = 2kL$ where k is the wavenumber of propagation in the medium. The FPI's reflected spectrum is used in the used system as a band filter.

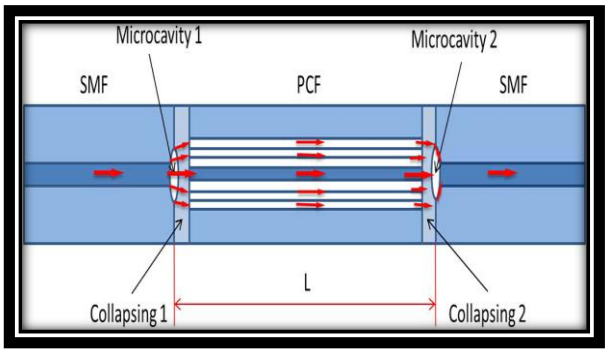

Fig. (4): Micro-cavity formation at the splicing point between SMF (on the left) and SCPCF (on the right) [16].

The periodicity of the channelled spectrum is given by [18]:

$$\Delta\lambda = m\frac{\lambda^2}{2n_{pcf}L_{pcf}} \quad (7)$$

At resonance wavelength λ_R , the phase difference is multiple of 2π. Hence,

$$\lambda_R = \frac{2\,n\,p\,Lpcf}{p} \quad (8)$$

Where p is an integer.

When the PCF segment is subjected to the external perturbations, λ_R is shifted by

$$\Delta\lambda_R = \left(\frac{\Delta n}{n} + \frac{\Delta L_{PCF}}{L_{PCF}}\right)\lambda p = \left(\frac{\Delta n_{eff}}{n_{eff}} + \varepsilon z,PCF\right)\lambda_R \quad (9)$$

Where Δn and ΔL_{PCF} are the changes in n and L_{PCF}, respectively. The Bragg wavelength shift can be

$$\Delta\lambda_B = (\frac{\Delta n_{eff}}{n_{eff}} + \frac{\Delta\Lambda}{\Lambda})\lambda_B = (\frac{\Delta n_{eff}}{n_{eff}} + \varepsilon z, FBG)\,\lambda_B \quad (10)$$

Where Δn_{eff} and $\Delta\Lambda$ are the changes in n_{eff} and Λ of FBG [18].

Experimental Procedure

Figure (5) and (6) show the schematic diagram and laboratory experimental components utilized to examine the performance of the proposed system. Light from a broadband light source (BBS) centered at 1550nm for illuminating the two micro-cavities embedded MZI-fiber Bragg grating. The reflected light signal from the micro-cavity interferometer was redirected by the circulator to the OSA for analysis and record. The detected spectrum is then sent to a personal computer for signal processing.

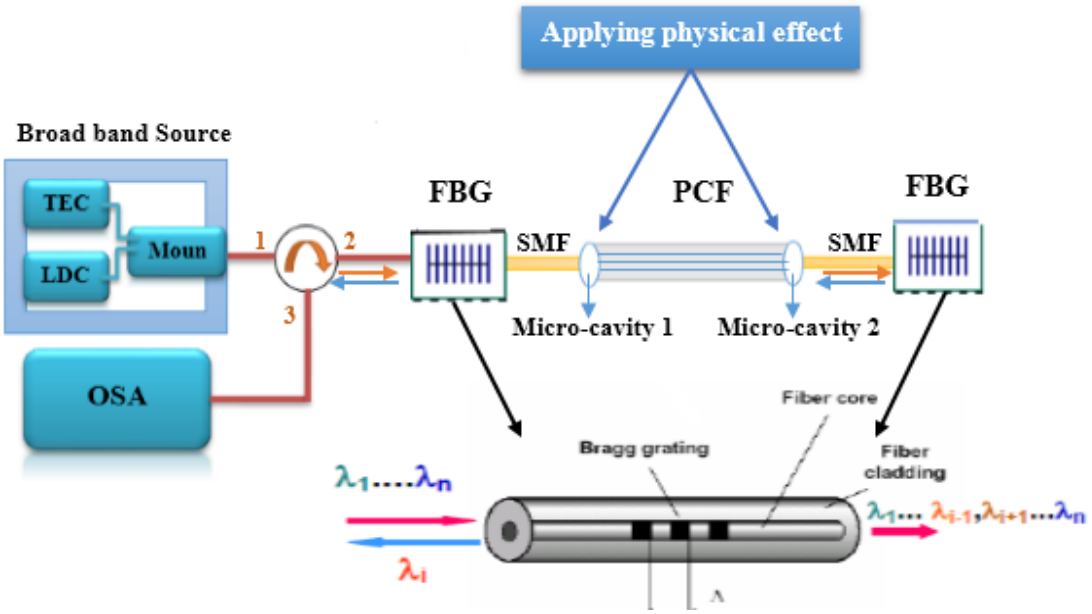

Fig. (5): Schematic diagram of a tunable band pass filter in-line micro-cavity MZI with physical effect system.

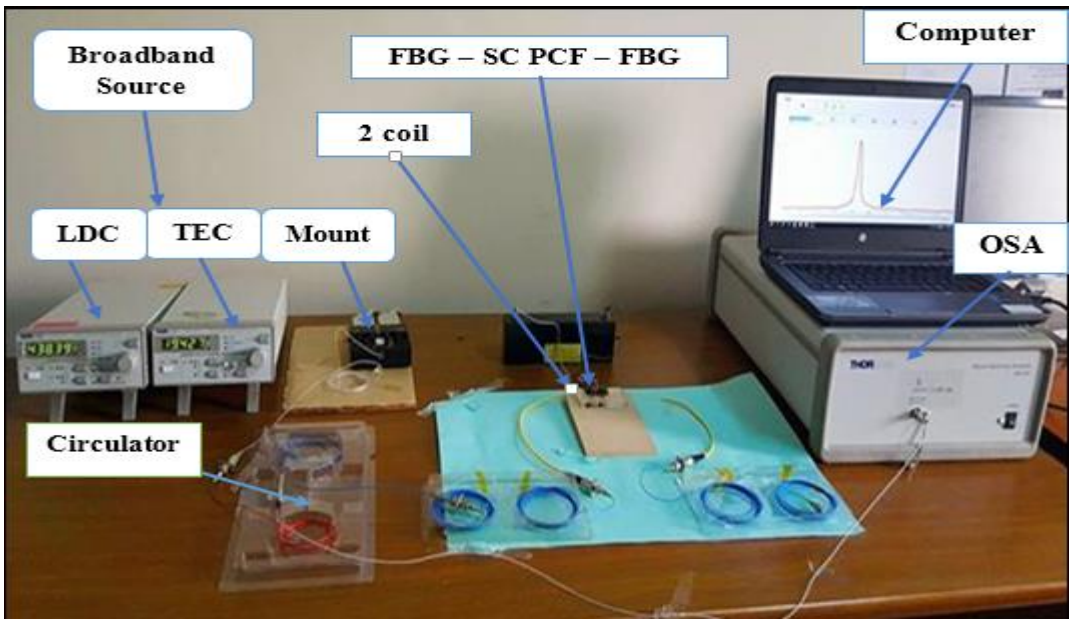

Fig. (6): The experimental setup for PCF-MZI Fabry Perot tunable Band pass filter with temperature effect

The optical spectrum of BBS extends from (1450) nm to (1650) nm. The maximum optical power of the BBS is (31.2) mW. The BBS consists of Ic chipset which is the basic element that generates the optical signal. Laser diode controller (LDC) gives the required power for the emitted optical signal. Temperature electric control (TEC) controls the emitted wavelengths and the optical output power. The specification of fibers used to fabrication micro-cavity interferometer SMF with LMA -10 was summarized in table (2) .In this work, we fabricated MZI with four micro- cavities (2 sensor) by fusion splicer .The arc time and arc power of the splicer are optimized such that the air holes having arbitrary shape is formed at the junction of SMF and PCF.

Table (2):SMF, NKT HC-1550 and NKT LMA-10 specification

Fiber name	Diameter µm			Pitch Λ	d_h/Λ
	Core d	Holes	Cladding D		
SMF	8.2	-	125 ± 2	-	-
LMA-10	10.1 ±0.5	3.38	125 ± 2	7.2	48%

Result and Discussion

The micro-cavity was constructed by fusion splicing of SCF (LMA-10) between equal spaces SMF and photographed with a microscope to determine the size and shape as shown in figure (7). The resulting output should be observed to confirm the changes in dimensions, Because of the variability in construction specific dimensions couldn't be controlled. The tunability of the geometrical parameters was accomplished by changing the length of SCPCF (LMA-10) and splicing parameters. The width of the micro- cavity is that the axis of the ellipsoid perpendicular to the core of the fiber in the range (24.92 to 62.32) µm while the length of the micro-cavities are parallel to the propagation axis of the fiber in the range of (3.82 to 18.2) µm as shown in table (3). This could be reduced volume of air at the splice joint in the micro-cavities produced. The dimensions of the micro-cavities was constructed by fusion splicer as summarized in Table (3).

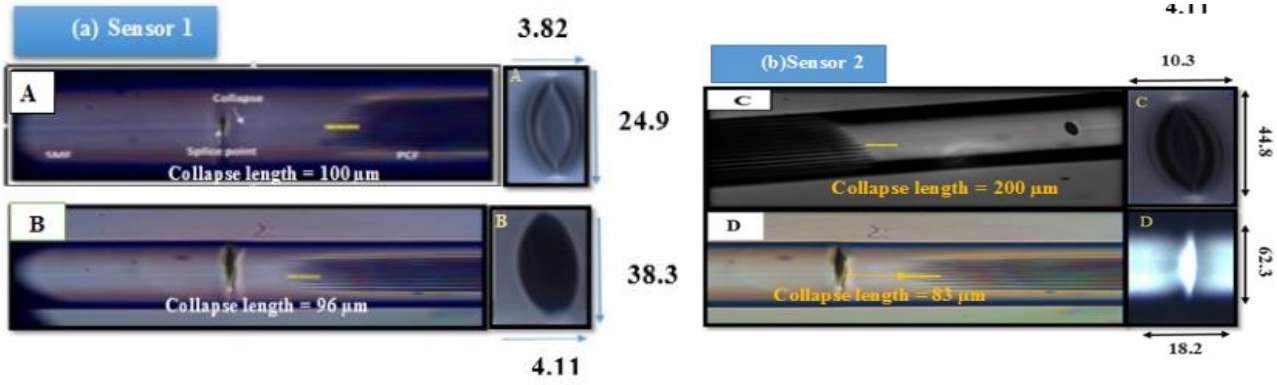

Fig. (7): Microscope images (a) Sensor 1 and (b): Sensor 2 in- Line MZI based on dual micro-cavity interferometer.

Table (3): The dimensions of the micro-cavities were constructed by fusion splicer.

Sensor name		PCF Length (cm)	Width(r) (µm)	Length(d) (µm)	Size of micro-cavity 10^3 (µm)
Sensor 1	**A**	3	24.92	3.82	3.807
	B	2.5	38.33	4.11	6.301
Sensor 2	**C**	2	44.85	10.3	18.478
	D	1.5	62.32	18.2	45.368

The relationship between length of the PCF sample and micro-cavities has been evaluated .It is found that there is a linear relation where any increase in the length of the PCF results in an increasing the size on the air micro-cavity [23]. This can be clearly shown in figure (8).

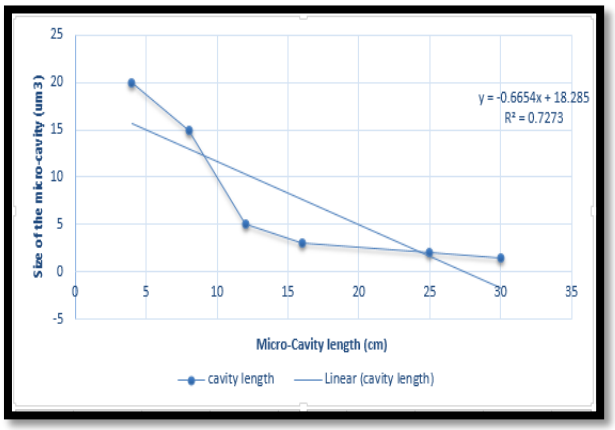

Fig. (8): Relation between the size of the micro-cavity and length of LMA-10

In this work the mode field mismatch between LMA-10 (MFD ≈10.1) and SMF (MFD ≈8.2). A specific method of splicing [17] is performed to achieve low splice loss in the SMF-LMA-SMF interferometer. The dip wavelength was varied by re-arcing the PCF-SMF splicing point at low arc power. The MZI with dual micro-cavity which was obtained from splicing insert between two identical FBG in the SMF-LMA- FBG configuration. A small change in the micro-cavity length between the two FBGs led to the variation of dip wavelength. Re-arcing was repeated several times until the dip is shifted to the desired position. The measured band-edge wavelengths (λ_{B1}, λ_{B2}) and resonance wavelength (λ_R) of the reflection spectrum at room temperature (T = 25 °C) are 1546.559, 1547.603, and 1546.734 nm. The parameter were summarized in table (4):

Table(4):The parameter of tunable band pass Filter Based on PCF- air micro-cavity Interferometer and FBG

	Operating wavelength (nm)	FWHM (pm)	Reflection power (nW)
λ_{B1}	1545.559	350.841	1.63
λ_R	1545.603	366.323	8.56
λ_{B2}	1545.734	234.303	6.85

Figure (9) shows that the two FBGs share the same center wavelength and the SCF (LMA-10) segment forms a cavity between the two grating reflectors. As a result, a narrow dip was formed within the reflection curve of the FBG. It's known as resonance wavelength.

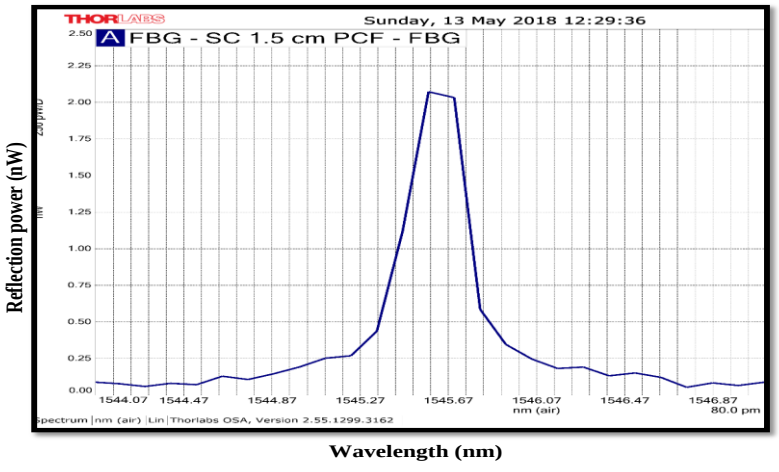

Fig. (9): Reflection spectrum of the proposed filter structure

The filter was tuning by splicing different length LMA-10 segment Contain the micro-cavity between two identical FBGs forming an FBG-PCF-FBG arrangement by controlling the fusion splicer parameters. It was appeared that the two FBGs that originate from the same uniform grating share the same center wavelength and the LMA-10 segment forms a cavity between the two grating reflectors. Therefore, a narrow dip was formed within the reflection curve of the FBG as shown in figure (10) .The characteristic of the reflection spectra is shown in table (5)

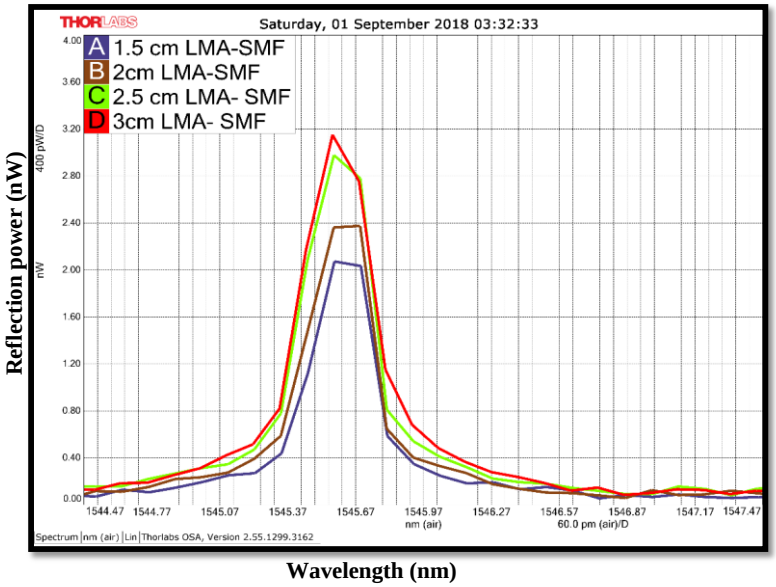

Fig. (10): Reflection spectrum of the proposed filter structure tuning by Re-arcing length of LMA-10.

Table (5): Characteristic of the reflection spectrum for different PCFs length contain the micro-cavity for FBG- PCF-FBG Filter			
Length PCF (cm)	**Resonance Wavelength (nm)**	**FWHM (pm)**	**Reflection Power (n W)**
1.5	1545.673	268.813	5.02
2	1545.600	399.720	5.12
2.5	1545.553	316.513	6.14
3	1545.546	370.619	8.67

Table (6): Characteristic of the reflection spectrum at different temperature degree			
Temperature (^{0}C)	**Centroid Wavelength (nm)**	**FWHM (pm)**	**Reflection Power (nW)**
Reference	1545.550	270.619	5.01
25	1545.580	310.916	6.30
35	1545.595	410.513	7.77
45	1545.622	398.720	8.43
55	1545.638	314.813	8.51

The response of the micro-cavity filter to temperature change is in the range of (25-55) ^{0}C. Figure (11) shows the obtained experimental results and the variation of dip wavelength resonance due to the small change in the micro-cavity length. The wavelength shift caused by a change in the phase difference between reflections from the two partially reflecting surfaces of the micro-cavity. This phase changes as the distance between these surface changes. The thermal expansion coefficient of silica glass is $10^{-6}/^0$C [18], which means that the distance between the surfaces experiences slight change with regards to temperature change. The thermal expansion of the cavity length plays important role in temperature sensitivity. The Characteristic of the reflection spectrum at different temperature was summarized in table (6):

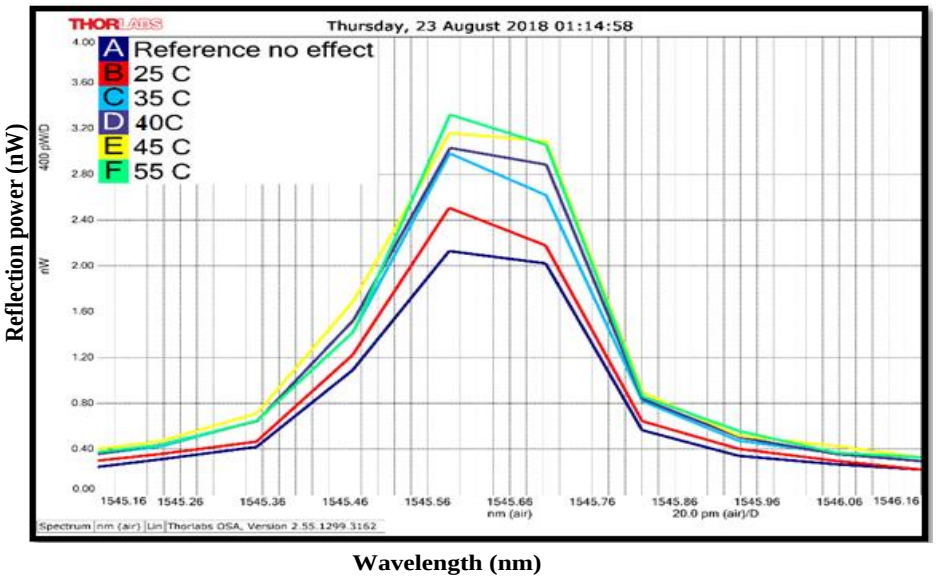

Fig. (11): Reflection spectrum of the proposed filter structure tuning by temperature change

When the temperature increase up to 20^{0}C the peak wavelength shift toward longer wavelength (red shift) because the interference pattern of the micro-cavity shift towards long wavelength region as you can see in figure (12) .The reflection spectra of a Fabry Perot resonator is dependent on the wavelength of the incident radiation. The interference was produced between the two FBGs produce standing waves which led to generate constructive interference when they will fit exactly with the cavity length.

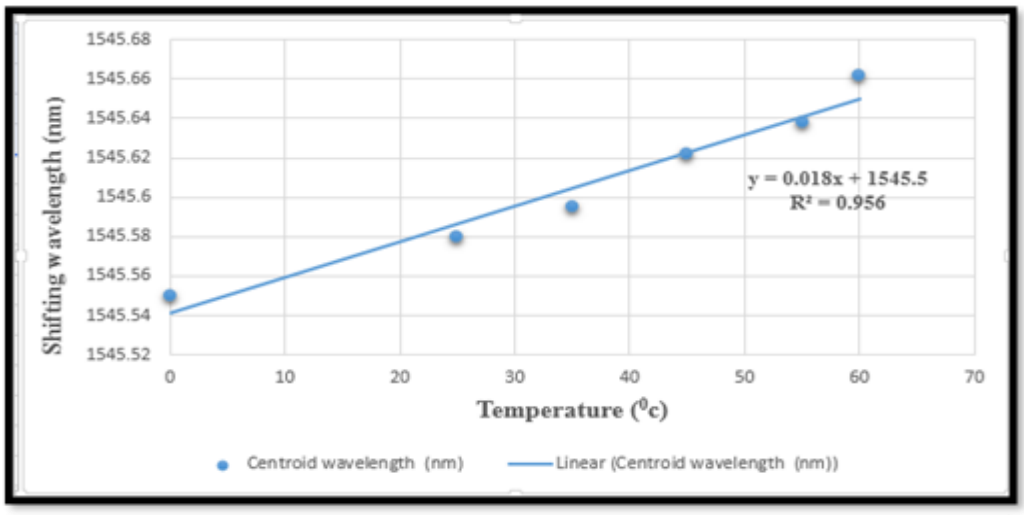

Fig. (12): The relationship between wavelength shift and temperature change.

The wavelength λ_{B1}, λ_{B2}, and λ_R have the same operating wavelength λ_c, therefore, the same sensitivity of ~ 18 pm/°C in the range of 25 - 55 °C was achieved for the proposed filter. The strain sensitivity of different dimension of the micro-cavity is 0.31nm as shown in figure (13):

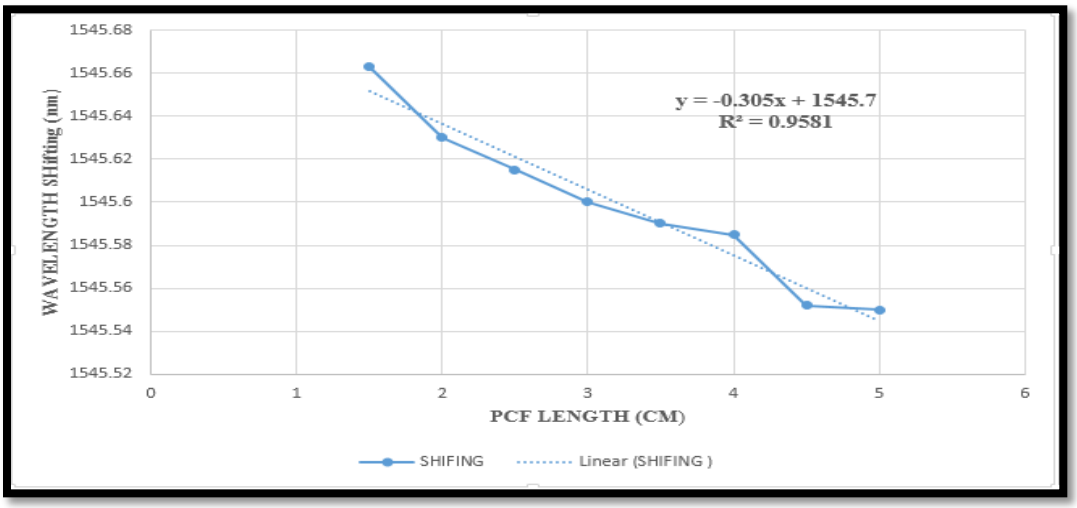

Fig. (13): the relationship between wavelength shift and length of PCF.

Conclusion

This paper proposed an inexpensive high contrast in-line micro-cavity interferometer for tunable band pass filter strain and temperature of micro-cavity region. The simulation model was presented in order to describe the sensor behavior which strongly agreed with the experimental results. The results showed evidences of high repeatability and stability achieved in measurements of strain and temperature from (3.82 to 18.2) μ Strain and 25°C to 55 °C, respectively.

Reference

[1] B. Culshaw, Optical fibre sensors: a current perspective, Open Optics J. 7 (1) (2013)21–31, http://dx.doi.org/10.2174/1874328501307010002

[2] B.H. Lee, Y.H. Kim, K.S. Park, J.B. Eom, M.J. Kim, B.S. Rho, H.Y. Choi, Interferometric fiber optic sensors, Sensors 12 (3) (2012) 2467–2486, http://dx.doi.org/10.3390/s120302467.

[3] K.O. Hill, G. Meltz, Fiber Bragg grating technology fundamentals and overview, J.Light. Technol. 15 (8) (1997) 1263–1276, http://dx.doi.org/10.1109/50.618320.

[4] D. Tosi, Advanced interrogation of fiber-optic Bragg grating and Fabry-Perot sensors with KLT analysis, Sensors 15 (11) (2015) 27470–27492, http://dx.doi.org/10.3390/s151127470.

[5] U. Tiwari, K. Thyagarajan, M.R. Shenoy, S.C. Jain, Edf-based edge-filter interrogation scheme for FBG sensors, IEEE Sens. J. 13 (4) (2013) 1315–1319, http://dx.doi.org/10.1109/JSEN.2012.2235064.

[6] D. Sengupta, P. Kishore, Continuous liquid level monitoring sensor system using fiber Bragg grating, Opt. Eng. 53 (1) (2014) 017102, http://dx.doi.org/10.1117/1.OE.53.1.017102.

[7] Q. Wu, Y. Semenova, A. Sun, P. Wang, G. Farrell, High resolution temperature insensitive interrogation technique for FBG sensors, Optics Laser Technol. 42 (4),pp. 653–656, (2010)

[8] G. Kouroussis, D. Kinet, E. Mendoza, J. Dupuy, V. Moeyaert, C. Caucheteur, Edge filter technique and dominant frequency analysis for high-speed railway monitoring with fiber Bragg gratings, Smart Mater. Structure. 25 (7) (2016) 075029

[9] Fujikura. Technical Datasheet: Fujikura (FSM-60S) Specialty Arc Fusion Splicer Manual. Technical report, Fujikura Corporation, 2012.

[10] Salah A. Adnan, Ahmed W. Abdulwahhab, Shymaa N. Ismail, *Fusion Splicing: the penalty of increasing the collapse length of the air holes in ESM-12B photonic crystal fibers*, Optical Applicata, vol XLVI, No. 2, 2016.

[11] C. Xiaopei, S. Fabin, W. Zhuang, H. Zhenyu, and A. Wang. Micro-air-gap based intrinsic Fabry-Perot interferometric fiber-optic sensor. Applied Optics,45: 7760-7766, 2006.

[12] M. Manders, M. Partridge, R. N. Correia, S. W. James, and R. P. Tatam. *Transverse strain response of in-fiber Fabry-Perot microcavities.* Proc. of SPIE, 9157:91571O, 2014.
[13] F. C. Favero, G. Bouwmans, V. Finazzi, J. Villatoro, and V. Pruneri. *Fabry Perot interferometers built by photonic crystal fiber pressurization during fusion splicing. Optics Letters, 36:4191- 4193, 2011.*
[14]L. Zhang, S. Sun, M. Li, and N. Zhu, "All-optical temporal fractional order differentiator using an in-fiber ellipsoidal air-microcavity," J. Semicond., vol. 38, no. 12, p. 126001, 2017.
[15] F. C. Favero, L. Araujo, G. Bouwmans, V. Finazzi, J. Villatoro, and V. Pruneri, Spheroidal Fabry-Perot microcavities in optical fibers for high-sensitivity sensing, Optics Express, 20(7):7112, 2012.
[16]Y. Wang, S. Wang, and L. Jiang, "Temperature-insensitive refractive index sensor based on Mach – Zehnder interferometer with two microcavities." Optics Letters, vol. 15, no. 2, p. 020-603,2017.
[17] C. A. R. Díaz *et al.*, "A cost-effective edge-filter based FBG interrogator using catastrophic fuse effect micro-cavity interferometers," *Meas. J. Int. Meas. Confed.*, vol. 124, no. 14, pp. 486–493, 2018.
[18] M. M. Ali, M. R. Islam, K. S. Lim, D. S. Gunawardena, H. Z. Yang, and H. Ahmad, "PCF-Cavity FBG Fabry-Perot Resonator for Simultaneous Measurement of Pressure and Temperature," *IEEE Sens. J.*, vol. 15, no. 12, pp. 6921–6925, 2015.
[19] M. Manders ,"Interferometric fiber optic sensors incorporating photonic crystal fiber for measurement of strain and load,"Cranfield university, M. Sc thesis, March, 2016.

تصميم وبناء مرشح تمرير النطاق البصري المستند على تجاويف الهواء للالياف البلوريه وفايبر براغ في مرنان فابيري بيروت

فراقد قاسم محمد تحرير منصور صفاء

معهد الليزر للدراسات العليا ، جامعة بغداد، بغداد، العراق

الخلاصة : تم تقديم مرشح تمرير النطاق المتباين المستند على مستشعر الليف من براغ باستخدام تجاويف الهواء الصغيره جدا في مقياس التداخل ماك- زندر .تكونت التجاويف بسب اللحام بين الالياف أحادية النمط وألياف الكريستال الضوئية بتقنية اللحام الكهربائي البسيطه. تم السيطره على اللحام من خلال التحكم بالعديد من العوامل منها قدرة اللحام وطول الالياف الكرستالية الصلبة والفجوه المتراكبة . تجويف الهواء ذو الشكل البيضوي بين الألياف كونت تجويف فابري-بيروت. وكانت خسارة الانعراج منخفضة للغاية بسبب طول التجويف القصير. تم تحقيق تجاويف متناهية الصغر تجريبيا بشكل موازٍ لمحور الانتشار ذي الأبعاد (24.92 - 62.32) مايكرومتر للعرض و (3.82 - 18.2) ميكرومتر للطول. تم تحقيق أقصى قدر من التباين 0.73 نانومتر عند الحد الأدنى لطول الليف من في المدى (1545.673-1545.546) نانو متر عندما كان حجم التجويف هو $45.36 * 10^3$ مايكرومتر . اعلى حساسيه كانت 0.31 نانومتر / سم وهي اعلى بكثير من حساسية الحرارة 18 بيكومتر /درجة مئوية.